Superparamagnetic Cobalt Ferrite Nanocrystals Synthesized by Alkalide Reduction

Kim E. Mooney, Jennifer A. Nelson, and Michael J. Wagner*

The George Washington University, Department of Chemistry, Washington, D.C. 20052

Received January 23, 2004. Revised Manuscript Received May 25, 2004

$CoFe_2O_4$ nanocrystallites have been synthesized by alkalide reduction of Co^{2+} and Fe^{3+} to form nanoscale $CoFe_2$, followed by oxidation with aerated water at room-temperature resulting in the nanocrystalline ferrite. As produced, the material consists of 2−4 nm nanocrystals that are superparamagnetic with an average blocking temperature of ∼350 K. Annealing at 100 °C in air results in a decrease in the blocking temperature to ∼250 K, with no detectable nanocrystallite growth. The dramatic change in the magnetic properties upon annealing is probably due to removal of crystal defects, namely oxygen vacancies. Further annealing to temperatures as high as 400 °C results in little change in the nanocrystallite size or the magnetic properties. Annealing at 500 °C results in the onset of significant growth in the nanocrystallite size, reaching 30 nm for material annealed at 1000 °C. The saturation magnetization, remanence, and squareness ratio, measured at 300 K, increase smoothly with increasing annealing temperature above 500 °C reaching 30 nm, 75 emu/g (94% of bulk value), 28 emu/g, and 0.37 respectively, for material that had been annealed at 1000 °C. The unannealed material has the largest coercivity observed in this study, 5.13 kOe at 5 K falling to 116 Oe at 300 K. The coercivity at 300 K declines dramatically to 0.9 Oe upon annealing at 100 °C, rising sharply to 67 Oe for material annealed at 500 °C, falling to 44 Oe for material annealed at 600 °C, and then steadily growing with increasing annealing temperature to 59 Oe for material annealed at 1000 °C. The anomalous increase in coercivity observed for samples annealed at 500 °C appears to be due to an increase in the average crystallite aspect ratio, which declines upon annealing at higher temperature.

Introduction

The properties of nanoparticulate magnetic materials depend strongly on the shape and size of the particles. In addition, the interaction between the particles can strongly influence their magnetic properties. The great interest in nanoparticulate materials in recent years is due to the potential to "tailor" their properties by the control of the size, shape, and interparticlate interactions.

Cobalt ferrite, $CoFe_2O_4$, crystallizes in an inverse spinel structure. In the bulk, it is ferrimagnetic with Curie temperature, T_c, of 790 K,[1] a moderate saturation magnetization (M_s = 80 emu/g),[2] high coercivity (H_c = 5.4 kOe),[3] high chemical stability, and wear resistance and is electrically insulating. The use of bulk $CoFe_2O_4$ in high-frequency applications is precluded by its large magnetocrystalline anisotropy,[4] which is principally due to the orbital angular momentum of the Co^{2+} ions, leading to large hysteresis losses[5] that may be overcome by reduction of crystallite size to the nanoscale regime. In addition, nanocrystalline $CoFe_2O_4$ is thought to be a promising material for high-density recording. These and other considerations have led to significant interest in nanocrystalline $CoFe_2O_4$ in recent years.[3,6−19] It is clear from these studies that the properties of nanocrystalline $CoFe_2O_4$, as is generally the case for magnetic materials, strongly depend

* To whom correspondence should be addressed. Phone: (202)994-6843. Fax: (202)994-2298. E-mail: wagnerm@gwu.edu.

(1) McCurrie, R. A. *Ferromagnetic Materials − Structure and Properties*; Academic: San Diego, 1994; p 123.
(2) Berkowitz, A.; Schuele, W. T. *J. Appl. Phys.* **1959**, *30*, 134S.
(3) Lee, J. G.; Park, J. Y.; Oh, Y. J.; Kim, C. S. *J. Appl. Phys.* **1998**, *84*(5), 2801−4.
(4) Jakubovics, J. P. *Magnetism and Magnetic Materials*; University Press: Cambridge, 1994; p 107.
(5) Stoppels, D. *J. Magn. Magn. Mater.* **1996**, *160*, 323.
(6) Blaskov, V.; Petkov, V.; Rusanov, V.; Martinez, L. M.; Martinez, B.; Munoz, J. S.; Mikhov, M. *J. Magn. Magn. Mater.* **1996**, *162*, 331.
(7) Masheva, V.; Grigorova, M.; Valkov, N.; Blythe, H. J.; Midlarz, T.; Blaskov, V.; Geshev, J.; Mikhov, M. *J. Magn. Magn. Mater.* **1999**, *196−197*, 128.
(8) Charles, S. W.; Chandrasekhar, R.; O'Grady, K.; Walker, M. *J. Appl. Phys.* **1988**, *64*(10), 5840.
(9) Koutani, S.; Gavoille, G. *J. Magn. Magn. Mater.* **1994**, *138*, 237.
(10) Tejada, J.; Ziolo, R. F.; Zhang, X. X. *Chem. Mater.* **1996**, *8*, 1784.
(11) Moumen, N.; Bonville, P.; Pileni, M. P. *J. Phys. Chem.* **1996**, *100*, 14410.
(12) Moumen, N.; Pileni, M. P. *Chem. Mater.* **1996**, *8*, 1128.
(13) Yan, C.-H.; Xu, Z.-G.; Cheng, F.-X.; Wang, Z.-M.; Sun, L.-D.; Liao, C.-S.; Jia, J.-T. *Solid State Commun.* **1999**, *111*, 287.
(14) Gajbhiye, N. S.; Prasad, S.; Balaji, G. *IEEE Trans. Magn.* **1999**, *35*(4), 2155.
(15) Rondinone, A. J.; Samia, A. C. S.; Zhang, Z. J. *J. Phys. Chem. B* **1999**, *103*, 6876.
(16) Liu, C.; Rondinone, A. J.; Zhang, Z. J. *Pure Appl. Chem.* **2000**, *72*(1−2), 37.
(17) Ammar, S.; Helfen, A.; Jouini, N.; Fievet, F.; Rosenman, I.; Villain, F.; Molinie, P.; Danot, M. *J. Mater. Chem.* **2001**, *11*, 186.
(18) Cabanas, A.; Poliakoff, M. *J. Mater. Chem.* **2001**, *11*, 1408.
(19) Hyeon, T.; Chung, Y.; Park, J. Y.; Lee, S. S.; Kim, Y.-W.; Park, B. H. *J. Phys. Chem.* **2002**, *106*, 6831.

10.1021/cm040012+ CCC: $27.50
Published on Web 07/10/2004

on the method of production. Thus, we have undertaken a study of nanocrystalline $CoFe_2O_4$ synthesized by alkalide reduction.

Alkalides are crystalline ionic salts consisting of crown ether or cryptand complexed alkali metal cations charged balanced by a stoichiometric number of alkali metal anions.[20,21] Alkalides produce alkali metal anions when dissolved in nonreducible solvents. The alkali metal anion is nearly as thermodynamically powerful a reductant as a solvated electron, the most powerful reductant possible in any given solvent and is capable of simultaneous two electron transfers. Alkalide reduction of metal salts results in the formation of a colloid of nanoscale particles. Colloid stability varies from minutes to hours, depending on the metal reduced and the reaction conditions. Following aggregation and removal of the solvent, the byproducts can be washed away, recovering the crown ether and leaving bare metal nanoparticles. Supported particles can be produced as well.[22−25]

Previous studies showed the general applicability of the alkalide reduction method to producing nanoparticles of elements from p-block semimetals to the early transition metals and even the rare earths.[22,23,25−28] The synthesis of carbides,[29,30] nitrides,[31] binary oxides of the early transition metals,[32] oxide phosphors,[33] and ternary oxide nanorods[34] as well as alloys and intermetallics[22,25,28] has been reported. Here we extend the method to the synthesis of a binary alloy followed by oxidation to form nanoscale particles of the ternary oxide, $CoFe_2O_4$.

Experimental Section

The nanoscale cobalt ferrite was synthesized by homogeneous alkalide coreduction of Fe^{3+} and Co^{2+} to form the nanoscale alloy followed by oxidation according to the following scheme:

$$4K^+(\text{15-crown-5})_2Na^- + 2FeCl_3 + CoI_2 \xrightarrow[-30\ °C]{THF}$$

$$CoFe_{2\ nano} + 4K(\text{15-crown-5})_2Cl_{0.5}I_{0.5} + 4NaCl$$

$$CoFe_{2\ nano} \xrightarrow{\text{aerated } H_2O} CoFe_2O_{4\ nano}$$

Physical and magnetic characterization of the precursor to $CoFe_2O_4$, nanoscale $CoFe_2$ alloy, will appear elsewhere. Note, the assignment of the I^- in the byproducts in the reaction scheme is based on the lack of observed NaI in X-ray patterns of unwashed samples; however, its inclusion in a mixed chloride/iodide crown ether complex phase is by no means certain. The lack of apparent gas evolution during the washing process is consistent with oxidation of the nanoparticles by dissolved O_2. Product yields averaged 96(3)% for the preparations performed for this study (note, the number in parentheses is the standard deviation). Reaction yield should be 100% given the overwhelming reduction potential of Na^-; however, in our small-scale synthesis (typically 0.15 g of $CoFe_2O_4$), a small percentage was lost in recovery, especially in the decanting stages.

Anhydrous CoI_2 (99.5%) was purchased from Alfa-AESAR, and $FeCl_3$ (97%) and $CoCl_2$ (97%) were purchased from Aldrich. These salts were used without further purification. Crown ether (15-crown-5, 98%) was purchased from Alfa-AESAR, further dried, and then purified by vacuum distillation. Tetrahydrofuran (THF, 99.9+% HPLC grade, inhibitor free) was purified by stirring over KNa alloy until a persistent blue solution was obtained. Water, used as the wash solvent, was distilled and then purified by filtration through a Barnstead E-pure system to a resistance of 18.3 MΩ/cm. All reactant manipulation was performed in a N_2 filled drybox (<1 ppm H_2O and O_2), and solvent transfers were accomplished by vacuum techniques (10^{-6} Torr). Sample annealing was done in Pt combustion boats for 4 h at the given temperature under ambient atmosphere. Infrared spectra were obtained with a Perkin-Elmer Spectrum RX FT-IR spectrometer. Elemental analysis was performed by flame emission spectroscopy using a Perkin-Elmer AAnalyst 100 spectrometer.

Electron micrographs were obtained on a JEM-1200EX transmissions electron microscope (TEM) operating at 80 keV. Samples for TEM were dispersed in MeOH by sonication and deposited on Formvar holey film/carbon coated copper grids. Powder X-ray patterns were obtained with a Scintag XDS-2000 diffractometer using Cu Kα radiation and a Peltier cooled solid-state detector.

Surface area measurements were made on a custom (in-house) built adsorption apparatus using the BET method with N_2 as the adsorption gas and the sample immersed in a liquid N_2 bath. The system is based on classical designs and uses two burets with 11 Hg filled bulbs to vary total volume. Pressure was measured with a MKS Instruments 870B capacitance manometer using a 660-B10 power supply/display. The vapor pressure of N_2 at adsorption temperature (P_o) was measured directly with a second Hg manometer. Samples that were annealed at temperatures between 200 and 400 °C were degassed for 8 h at 200 °C under vacuum (10^{-6} Torr) prior to adsorption measurements. Those annealed at higher temperatures were degassed in a similar manner but for a shorter time (4 h) and at a higher temperature (400 °C).

Magnetic characterization was performed with a Quantum Design model MPMS-XL5 SQUID magnetometer. The magnet was reset prior to sample cooling in the absence of an applied field (ZFC) to minimize the residual field present. Magnetization measurements of ZFC and FC (field cooled) samples were obtained with increasing temperature. Samples, in the form of packed powders, were vacuum-sealed (10^{-6} Torr) in high field NMR tubes and placed butt to butt with an empty, vacuum-sealed NMR tube in a sample straw to minimize background diamagnetism.

Results and Discussion

Following washing, the product is a black, free-flowing powder that responds easily to a magnet. Powder X-ray diffraction (XRD) patterns of the material show broad peaks consistent with cubic $CoFe_2O_4$ (JCPDS PDF #221086). $CoFe_2O_4$ stoichiometry (metals basis) was confirmed by flame emission spectroscopy. FT-IR spec-

(20) Wagner, M. J.; Dye, J. L. *Annu. Rev. Mater. Sci.* **1993**, *23*, 223.
(21) Wagner, M. J.; Dye, J. L., Alkalides and Electrides. In *Comprehensive Supramolecular Chemistry*; Lehn, J. M., Gokel, G. W., Eds.; Elsevier: Oxford, U.K., 1996; Vol. 1, p 477.
(22) Tsai, K.-L.; Dye, J. L. *J. Am. Chem. Soc.* **1991**, *113*, 1650.
(23) Tsai, K. L.; Dye, J. L. *Chem. Mater.* **1993**, *5*, 540.
(24) Cowen, J. A.; Tsai, K. L.; Dye, J. L. *J. Appl. Phys.* **1994**, *76*(10), 6567−6569.
(25) Dye, J. L.; Tsai, K. L. *Faraday Discuss.* **1991**, *92*, 45.
(26) Nelson, J. A.; Bennett, L. H.; Wagner, M. J. *J. Am. Chem. Soc.* **2002**, *124*(12), 2979.
(27) Nelson, J. A.; Bennett, L. H.; Wagner, M. J. *J. Mater. Chem.* **2003**, *13*, 857.
(28) Nelson, J. A. Synthesis and Characterization of Nanomaterials by Alkalide Reduction, Ph.D. Thesis, The George Washington University, Washington, DC, 2002.
(29) Nelson, J. A.; Wagner, M. J. *Chem. Mater.* **2002**, *14*, 1639.
(30) Nelson, J. A.; Wagner, M. J. *Chem. Mater.* **2002**, *14*, 4460.
(31) Chen, X. Z.; Dye, J. L.; Eick, H. A.; Elder, S. H.; Tsai, K.-L. *Chem. Mater.* **1997**, *9*, 1172.
(32) Nelson, J. A.; Wagner, M. J. *Chem. Mater.* **2002**, *14*(2), 915.
(33) Nelson, J. A.; Brant, E. L.; Wagner, M. J. *Chem. Mater.* **2003**, *15*, 688.
(34) Nelson, J. A.; Wagner, M. J. *J. Am. Chem. Soc.* **2003**, *125*, 332.

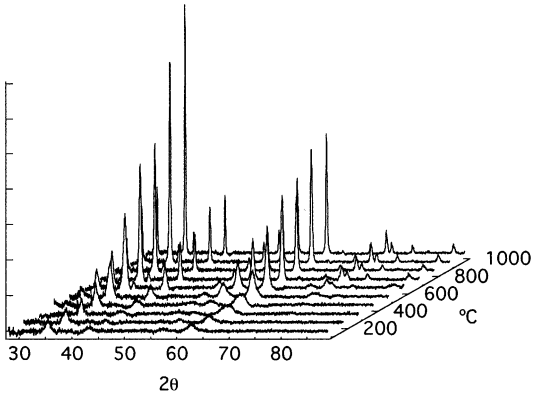

Figure 1. Powder diffraction patterns of $CoFe_2O_4$ nanocrystals heated for 4 h at the indicated temperature.

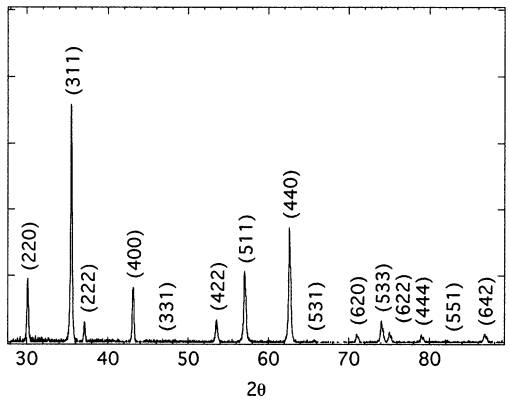

Figure 2. Powder diffraction patterns of $CoFe_2O_4$ nanocrystals after heating to 1000 °C for 4 h with the Miller indices indicated above the reflections (JCPDS PDF #221086).

tra of the material showed it to be free of organic byproducts.

Annealing the material in air causes the XRD peaks to sharpen, indicative of crystallite growth (Figure 1). We could detect no other crystalline phases in the XRD patterns (Figure 2). The average crystallite size of the unannealed material, as determined from XRD line broadening, depends on the cobalt salt used for the reaction: syntheses employing CoI_2 resulted in average crystallite sizes of ~3 nm, while those made with $CoCl_2$ exceeded 7 nm. Samples made with CoI_2 were used for this study.

The average crystallite size increases with increasing temperature from 3.1 to 30.2 nm for unannealed samples and those annealed at 1000 °C, respectively (Figure 3). The growth is modest below 400 °C, increasing at an average of <0.5 nm/100 °C. Above 400 °C, the growth is far more dramatic: the average crystallite size increases by >4 nm/100 °C. Surface area measured by the BET method, 198 m^2/g for materials heated to 200 °C for 8 h (to outgas prior to measurement), decreases steadily with annealing temperature to 7 m^2/g for those annealed at 1000 °C, consistent with the increase in crystallite size.

TEM micrographs of the unannealed samples show them to consist of agglomerated 2−4 nm nanocrystals of rough, irregular but generally spheriodal shape (Figure 4), consistent with the crystallite size found by powder XRD. Quantitative measurement of the size distribution is complicated by the agglomeration of these magnetic nanocrystallites, making it somewhat difficult

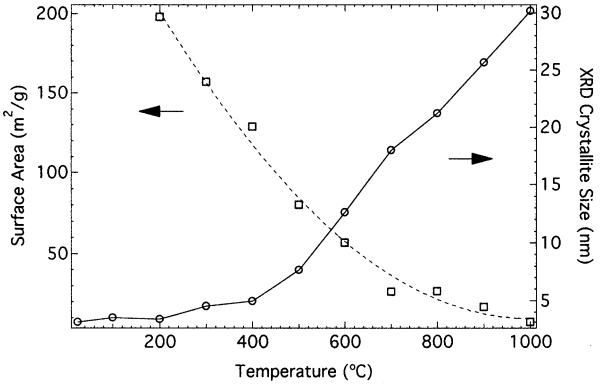

Figure 3. Suface area (squares, left axis), determined by BET adsorption measurements, and the average crystallite size (circles, right axis), determined from the XRD line broadening of the (311), (440), and (511) reflections, as functions of annealing temperature. The lines connecting the data points are to guide the eye.

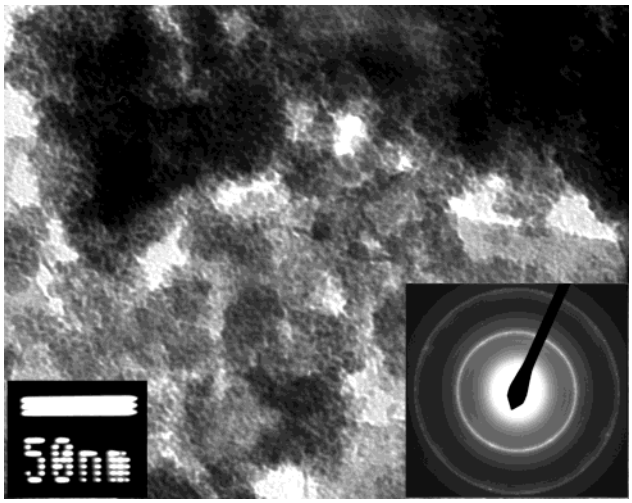

Figure 4. TEM micrograph of $CoFe_2O_4$ nanocrystals as prepared at room temperature. Inset is an electron diffraction pattern on the sample. All 11 reflection circles visible in original film can be indexed, matching those expected for crystalline $CoFe_2O_4$.

to distinguish individual nanocrystallites in bright field images. However, close inspection of the micrographs revealed that the distribution is narrow: the vast majority of the distinguishably individual nanocrystals have diameters of 2−3 nm (largest dimension), and none were found to exceed 5 nm. Selected area electron diffraction (SAD) patterns confirm the XRD phase identification, with more than 11 diffraction rings discernible, all of which can be indexed to cubic $CoFe_2O_4$ (JCPDS PDF #221086). Annealing the material results in a growth in observed particle size, consistent with XRD observations. The shape of the nanocrystals annealed between 100 and 400 °C is somewhat less regular than that observed in the unannealed material. Further annealing of the nanocrystals at 500 °C results not only in visible particle growth but also many particles that have an increased aspect ratio, seemingly due to the joining of 2 or more nanocrystallites (Figure 5). Annealing at temperatures exceeding 500 °C results in visibly smoother, more "rounded" particles that are somewhat less apt to agglomerate with an increasing number of nanocrystals exhibiting what appear to be facets as the annealing temperature is increased (Figure 6).

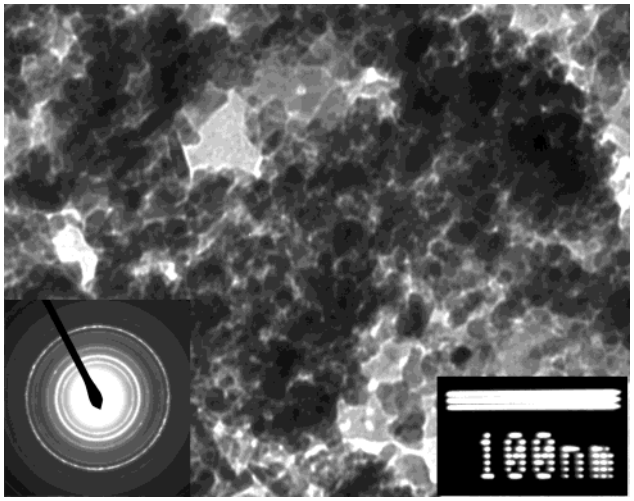

Figure 5. TEM micrograph of $CoFe_2O_4$ nanocrystals after annealing in air at 500 °C for 4 h. Inset is an electron diffraction pattern on the sample, matching that expected for crystalline $CoFe_2O_4$.

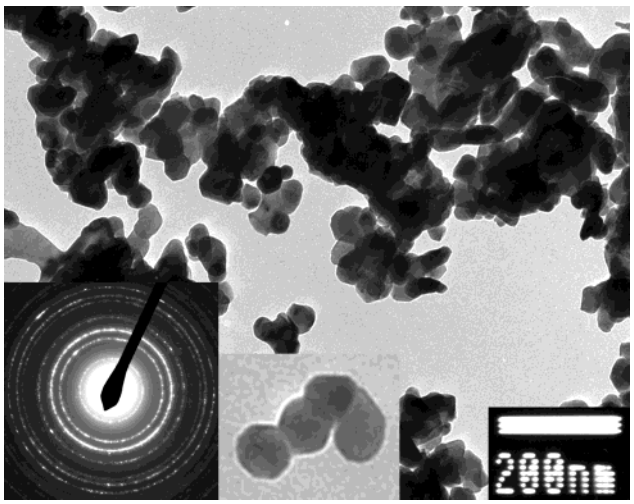

Figure 6. TEM micrograph of $CoFe_2O_4$ nanocrystals after annealing to 1000 °C for 4 h. The "streaking" across the nanocrystals (diagonally, lower left to upper right) seen on the micrograph is due to magnetic interaction of the electron beam with the sample. Inset to the left is an electron diffraction pattern of the sample matching that expected for crystalline $CoFe_2O_4$. Inset in the center is an isolated group of nanocrystals magnified at an additional 3× showing the appearance of facets.

The temperature dependence of the magnetization of unannealed $CoFe_2O_4$ nanocrystals cooled in the absence (ZFC) of, and in the presence (FC) of, an applied field is shown in Figure 7. The ZFC magnetization rises with increasing temperature, reaching a maximum (T_{max}) at ~350 K. The FC magnetization is at its maximum at low temperature, falling steadily until it converges with the ZFC data at ~375 K.

The isothermal magnetic field dependence of the magnetization of unannealed $CoFe_2O_4$ nanocrystals at 5 and 300 K are shown in Figure 8. At 5 K, the sample exhibits hysteric behavior typical of ferrimagnetism, with coercivity, H_c, of 5.13 kOe, remanence, M_r, of 29.3 emu/g, and saturation magnetization, M_s, of 50.1 emu/g, obtained by extrapolating a graph of M vs $1/H$ to $1/H = 0$. The squareness (remanence) ratio, M_r/M_s, is 0.59, larger than that expected for noninteracting, randomly

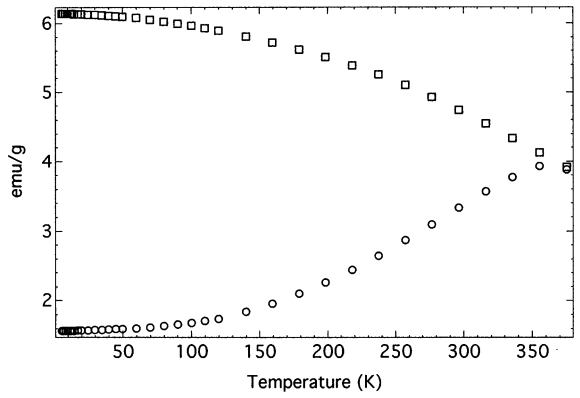

Figure 7. Temperature dependence of the magnetic susceptibility of unannealed $CoFe_2O_4$ nanocrystals cooled in the absence (circles) and presence (squares) of a 100 Oe applied field.

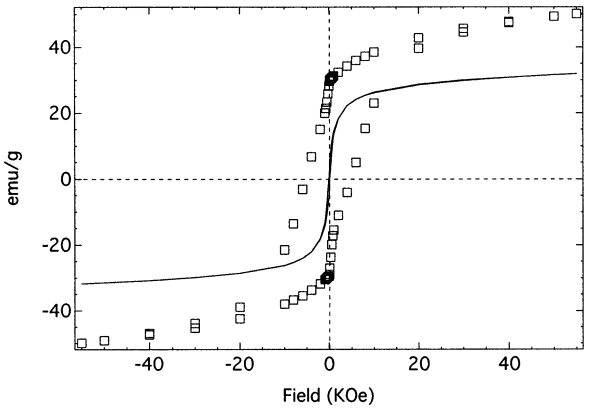

Figure 8. Magnetization loops for unannealed $CoFe_2O_4$ nanocrystals obtained at 5 K (squares) and 300 K (solid line).

oriented, uniaxial single domain particles (0.5)[35] and smaller than that expected for particles with cubic anisotropy (0.83).[8] Considering that $CoFe_2O_4$ exhibits strong cubic magnetocrystalline anisotropy in the bulk, one might expect cubic anisotropy; however, for 3 nm nanocrystals, more than 90% of the volume is within one unit cell length of the surface. Thus, it is likely that magnetocrystalline anisotropy does not dominate; shape, stress, and surface effects could all make significant contributions. In addition, considering the sample is insulating, significant interparticle superexchange interactions may exist in our packed powder samples.[36] Thus, it is possible that the overall anisotropy is uniaxial, as found by other investigators for similar sized nanocrystals.[11] The nearly 20% remanence enhancement we observe, as compared to that expected for noninteracting, randomly oriented, uniaxial single domain particles, could be due to interparticle exchange interactions.[35]

The magnetization loop measured at 300 K displays a markedly smaller coercivity (116 Oe) and remanence (3.1 emu/g) and a saturation magnetization reduced by nearly 40% (32.9 emu/g). The dramatic reduction in H_c and M_r, considered together with the convergence of the ZFC and FC magnetization data (Figure 7) more than

(35) Schrefl, T.; Fidler, J.; Kronmuller, H. *Phys. Rev. B* **1994**, *49*(9), 6100.

(36) Dormann, J. L.; Fiorani, D.; Tronc, E. Magnetic Relaxation in Fine-Particle Systems. In *Advances in Chemical Physics*; Prigogine, I., Rice, S. A., Eds.; John Wiley & Sons: 1997; Vol. XCVIII, p 283.

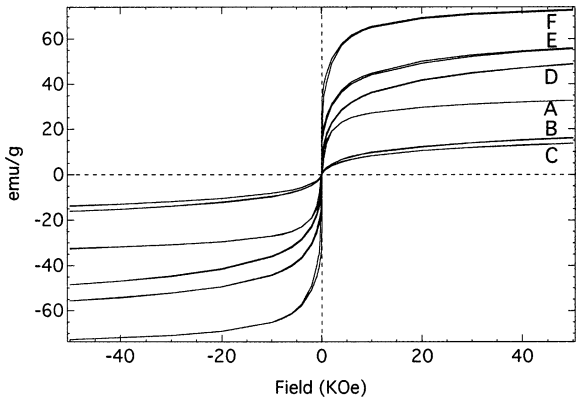

Figure 9. Isothermal magnetization loops obtained at 300 K for unnannealed (A), 200 °C (B), 400 °C (C), 600 °C (D), 700 °C (E), and 1000 °C (F) annealed $CoFe_2O_4$ nanocrystallites.

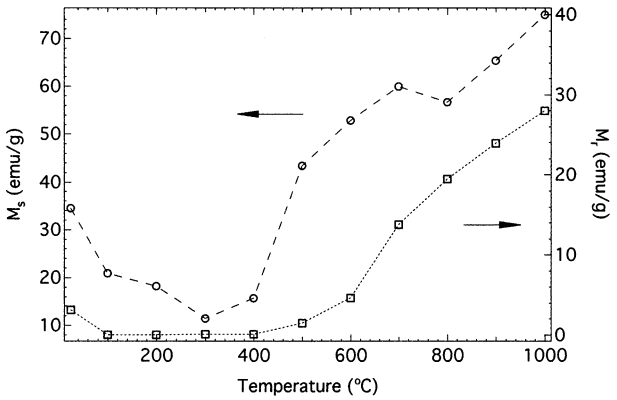

Figure 10. Saturation magnetization (circles, left axis) and remanence (squares, right axis) measured at 300 K for $CoFe_2O_4$ nanocrystals as a function of annealing temperature. Lines connecting data points are to guide the eye.

400 K lower than the bulk Curie temperature ($T_c = 790$ K),[1] is indicative of the onset of superparamagnetism.[37]

Isothermal magnetization loops, obtained at 300 K, for samples annealed at temperatures up to 1000 °C, are shown in Figure 9. Data were obtained for samples annealed in 100 °C increments; however, some of the loops are omitted for graphical clarity. In Figure 10, it can be seen that M_s declines by more than 40% following annealing at 100 °C. Increasing the annealing temperature results in a more moderate decline up to 400 °C, a sharp increase at 500 °C, and a fairly steady increase in M_s above that temperature, reaching 74.9 emu/g, or ~94% of the bulk value of 80 emu/g,[2] after annealing at 1000 °C. M_r, which decreases from 3.1 to 0.005 emu/g upon annealing to 100 °C (Figure 10), and the squareness ratio (Figure 11) follow similar trends. H_c also displays a marked decrease following annealing at 100 °C, from 116 to 0.9 Oe, and then increases modestly with increasing annealing temperature to 400 °C (Figure 11). The observed coecivity for our material after annealing to 100 °C is an order of magnitude lower than that observed in dry powders of similar size produced in microemulsions.[12] Annealing at 500 °C results in a spike in the coercivity to 67 Oe, falling to 44 Oe following annealing at 600 °C and increasing fairly steadily with increasing annealing temperature thereafter.

The dependence of the thermoremanent magnetization (TRM)[38] on temperature of the unannealed and

(37) Bean, C. P.; Livingston, J. D. *J. Appl. Phys.* **1959**, *30*(4), 120S.

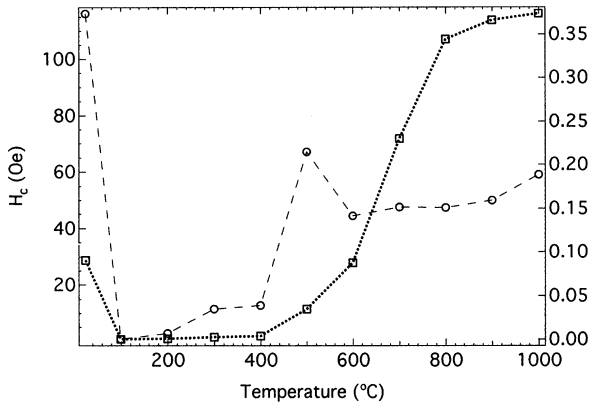

Figure 11. Coercivity (circles, left axis) and squareness ratio (squares, right axis) measured at 300 K for $CoFe_2O_4$ nanocrystals as a function of annealing temperature. Lines connecting data points are to guide the eye.

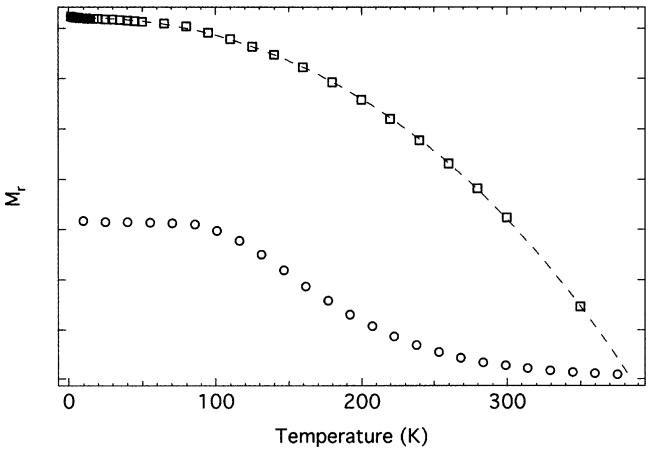

Figure 12. Temperature dependence of the thermoremanent magnetization for unannealed (squares) and 100 °C annealed (circles) $CoFe_2O_4$ nanocrystals. The annealed data have been scaled by multipling by a factor of 3 for better clarity. The line connecting the unannealed data is the fit used to extrapolate the thermoremanence to zero.

annealed $CoFe_2O_4$ nanocrystals is shown in Figure 12. These data were obtained by cooling the sample to 5 K in the presence of an applied field (100 Oe), removing the field, and measuring the remanent magnetization with increasing temperature. At any given temperature, only those particles that are blocked, those for which the energy barrier to the rotation of their magnetic moments cannot be overcome by thermal energy during the measurement time, contribute to the remanence. A distribution of blocking temperatures exists as a consequence of the distribution of anisotropy energies due to the finite crystallite size and shape distribution as well as interparticle interactions in the packed powder. Thus, as the temperature is increased, thermal energy becomes sufficient to overcome the anisotropy energies of progressively more crystallites and the remanence decreases.

The TRM of the unannealed $CoFe_2O_4$ nanocrystals decreases smoothly as temperature increases, approaching zero at ~380 K (extrapolated), the irreversibility temperature, T_{IRR}, above which the entire sample is able

(38) Fiorani, D. In *Static and Dynamic Properties of Superparamagnetic Particles*; Proceedings of the National School "New Developments and Magnetism's Applications", Naples, Italy, 1995, Oct 23–28, p 132.

to relax in the time scale of measurement. Whereas T_{max} of the ZFC magnetization curve (Figure 7) is a measure of the average blocking temperature, $\langle T_B \rangle$, of the sample, T_{IRR} is a measure of the sample's largest blocking temperature, above which the entire sample is in the superparamagnetic regime.[38] The convergence of the ZFC and FC measurements is another measure of T_{IRR} and is in good agreement with our TRM measurements. Also shown in Figure 12 is the TRM measurement for a sample annealed at 100 °C. It is clear from this measurement that annealing results in a decrease in T_{IRR} and thus T_B by ~100 K.

The reductions of M_s, M_r, H_c, and T_B observed with little or no increase in crystallite size upon annealing the nanocrystals to 100 °C are probably due to the reduction of crystal defects (oxygen deficiency). The nanocrystals made for this study result from the oxidation of alloy particles under very mild conditions. The production of ferrites by the oxidation of particles has been shown to result in incomplete oxidation of the core, leading to large stress anisotropy and coercivity enhancement.[39] Even point defects can significantly impede the growth of reverse domains and thus result in significant H_c enhancement in materials with a large anisotropy constants, such as $CoFe_2O_4$.[40] The incomplete oxidation of the nanocrystalline core could also result in incomplete ferrimagnetic ordering and therefore enhanced M_s and M_r, as observed.

The additional stress anisotropy due to incomplete oxidation of the nanocrystalline core could account for the high T_B observed in the unheated material. For noninteracting particles with uniaxial anisotropy, the energy barrier associated with magnetic reversal can be related to the anisotropy constant, K, and volume, V, by

$$E_B = KV$$

and K is directly proportional to the blocking temperature, T_B,

$$K = 25k_BT_B/V$$

where k_B is the Boltzman constant and V is the particle volume.[41] Calculating an "effective" anisotropy constant using $\langle T_B \rangle$ yields values of 6.5×10^7 erg cm^{-3} and 4.7×10^7 erg cm^{-3} for the unannealed and samples annealed at 100 °C, repectively. These values are significantly larger than the bulk $CoFe_2O_4$ anisotropy constant ($1.8-3.0 \times 10^6$ erg cm^{-3}).[42] The difference between the anisotropy constant calculated for the unannealed and annealed material is likely a measure of the additional stress anisotropy due to incomplete oxidation of the particle cores. The discrepancy between the anisotropy constant calculated for our annealed samples and bulk material is likely, in large part, due to strong interparticle interactions, via dipolar and exchange mechanisms.

The onset of significant crystallite growth when the annealing temperature is increased to 500 °C is accompanied, as one might expect, by an increase in M_s and M_r (Figure 10). In addition, there is a significant increase in $\langle T_B \rangle$, to 311 K, and a decrease in the apparent anisotropy constant, K, to 4.6×10^6 erg cm^{-3}, close to the bulk value and that observed for similar sized $CoFe_2O_4$ nanocrystals made by a surfactant route.[19] The decrease in K may be caused by a decrease in interparticle interactions due to the decrease in surface area and interparticle contact. Larger particles not only have less surface area to interact; the fraction of the surface area in contact with other particles decreases due to less efficient packing.

The increase in coercivity observed for material annealed at 500 °C and higher might be expected due to both nanocrystallite growth and the rise in blocking temperature above 300 K, the temperature at which the magnetization loops were measured. However, annealing at 500 °C causes H_c to grow anomalously (and reproducibly) large, decreasing upon further annealing to higher temperature (Figure 11). If the increase in H_c were due only to the increase in nanocrystallite size and blocking temperature, H_c would not decrease upon annealing to higher temperature, which results in additional nanocrystal growth. One explanation for the observed excessive increase in H_c is an increase in the nanocrystallites average aspect ratio upon raising the annealing temperature from 400 to 500 °C as indicated by TEM observations. Very small increases in the aspect ratio can lead to large changes in coercivity.[41] The decline in H_c upon higher temperature annealing could be the result of additional growth of the nanocrystals and the increased atomic mobility at higher annealing temperatures, resulting in an overall decrease in the aspect ratio, a "rounding" of the nanocrystals. Alternatively, one cannot rule out the possibility that magnetization pinning defects were incorporated into the nanocrystallites upon onset of significant crystallite growth at 500 °C, perhaps due to lattice mismatch between the intergrowing nanocrystallites. Annealing at higher temperature would reduce these defects and result in the decrease in H_c observed. The fairly steady increase in H_c, M_s, M_r, and squareness ratio with increasing annealing temperature between 600 and 1000 °C is consistent with the steady increase in crystallite size.

Conclusions

Nanocrystalline $CoFe_2O_4$ can be synthesized by mild oxidation of the nanoscale bimetallic alloy $CoFe_2$ made by alkalide reduction. The initial nanocrystallite size depends on the cobalt salt used in the reduction: reducing $CoCl_2$ results in nanocrystallites that are approximately twice as large as those made using CoI_2. As produced, the nanocrystallites are probably oxygen deficient. These crystal defects can be removed with no detectable nanocrystallite growth by annealing at 100 °C in air, resulting in a dramatic decrease in the superparamagnetic blocking temperature. Annealing in air allows one to modify the average particle size and magnetic properties. The saturation magnetization at 300 K reaches a maximum of 94% of the bulk value following annealing at 1000 °C, with very low coercivity, both desirable traits for high-frequency soft magnetic applications.

(39) Tailhades, P.; Bonningue, C.; Rousset, A.; Bouet, L.; Pasquet, I.; Lebrun, S. *J. Magn. Magn. Mater.* **1999**, *193*, 148.
(40) Livingston, J. D. *J. Appl. Phys.* **1981**, *53*(3), 2544.
(41) Lieslie-Pelecky, D. L.; Rieke, R. D. *Chem. Mater.* **1996**, *8*, 1770.
(42) Buschow, K. H. J. *Handbook of Magnetic Materials*; Amsterdam: 1995; Vol. 8, p 212.

Acknowledgment. The authors thank Dr. Robin Rufner and the George Washington University Center for Microscopy and Image Analysis for assistance and use of the TEM imaging facilities. In addition, we thank Dr. Robert Shull and the Magnetic Group at NIST for their assistance and access to their magnetometer. Finally, we thank the National Science Foundation for financial support (DMR-9876164).

CM040012+